Title
High-resolution geochemical record of Petaluma Marsh from the San Francisco bay area

Author
Fard, Elizabeth

Publication Date
2018

Peer reviewed|Thesis/dissertation

UNIVERSITY OF CALIFORNIA

Los Angeles

High-resolution geochemical record of Petaluma Marsh from the San Francisco bay area

A thesis submitted in partial satisfaction

of the requirements for the degree Masters of Arts

in Geography

by

Elizabeth Fard

2018

ABSTRACT OF THE THESIS

High-resolution
geochemical record of Petaluma Marsh from the
San Francisco bay area

by

Elizabeth Fard

Master of Arts in Geography
University of California, Los Angeles, 2018
Professor Glen Michael MacDonald, Chair

The San Francisco Bay has the largest concentration of salt marshes in the state of California, representing a diversity of marsh habit. Protecting these environments is critical, as salt marshes provide refuge to endangered species, absorb carbon from the atmosphere, and preserve detailed evidence of past climatic, hydrologic, geomorphic, and ecologic conditions. However, much of the marshes have been impacted by pollutants, altered or lost entirely due to human activity over the past 150 years, making their prehistoric conditions, ecological trajectories and resilience to disturbance uncertain. In this study, I collected data from Petaluma Marsh, one of the oldest marshes in the Bay Area, to document the geochemical changes including heavy metal concentrations as a response to climatic and anthropogenic changes since

the mid-Holocene. Loss-on ignition, pXRF, and magnetic susceptibility data were collected at high resolution from a 12-meter, 6109-year-old, sedimentary core recovered from this tidal marsh located along the Petaluma river in the northern Bay region. Average rate of sediment accretion is 3.6 mm yr-1 ± 0.8. Our results show that the introduction of European land-use and activities over the last 150-200 years resulted in disturbance of marsh biota and increases in heavy metals with unprecedented levels of lead and zinc. However, based on statistical time-series analysis of long-core elemental concentrations, results show that modern geochemical conditions are not so far removed compared to prehistoric conditions, as often suggested by century-scale analyses. Modern heavy metal concentrations (e.g., Cr, Fe, Sr, Ba, Zr, Rb and Ni) match concentration levels from 4000-6000 YBP. However, Pb levels in the marsh post-European land use are dramatically higher now than ever before. Our results show the effects of anthropogenic changes on this ancient and ecologically important marsh in the north San Francisco Bay area that can help better inform restoration ecologists and policy makers, specifically in terms of heavy-metal pollutants.

The thesis of Elizabeth Fard is approved.

Richard F. Ambrose

Thomas Welch Gillespie

Glen Michael MacDonald, Committee Chair

University of California, Los Angeles

2018

Table of Contents

List of Figures

List of Tables

ACKNOWLEDGEMENTS

I would like to acknowledge my advisor Glen M. MacDonald for his guidance. I would also like to thank Richard F. Ambrose and Thomas W. Gillespie. Lauren Brown has guided me through lab work, field work, research and life as a grad student. I owe much of my success to her. Simona Avnaim-Katav, Marcus Thomson, and Scott Lydon, have also provided professional and personal support to make this work possible.

Introduction

Research shows that humans have impacted or destroyed wetlands by activities such as farmland acquisition, introduction of non-native species, alteration of coastal hydrology, metal and nutrient pollution, and alteration of sediment delivery and subsidence rates (Bruland et al., 1974; Gedan et al., 2009; Kennish, 2001; Kirwan & Megonigal, 2013; Hornberger et al., 1999; Bai et al., 2011, Zhang et al., 2013). Heavy metal pollution in estuarine environments has been long been considered a threat to ecosystem health that is increasingly recognized as determental (Zhang et al., 2013; Connor & Thomas, 2003; Hornberger et al., 1999; Valette-silver, 1993; Daskalakis & Connor, 1995; Williams et al., 1994; Hornberger et al., 1999; Zhang et al., 2013).

San Francisco Bay coastal habitats, with their formerly vast region of marsh, have been affected by heavy metal pollution since the gold rush and subsequent industrial boom commencing in the 1850s (Luoma et al., 1998; Ritson et al., 1999). The Gold Rush of the 1850s instantly propelled San Francisco into an industrial urban mecca, attracting tens of thousands of people within a decade, with the population today around 10 million (Gilbert, 1917; Luoma et al., 1998; Walker, 2001; Ritson et al., 1999). With this boom in urbanization came huge expansion in manufacturing and agriculture (Walker, 2001). A byproduct of this expansions was an increase of heavy metals and other pollutants produced from mining practices, industrial activity, transportation, municipal waste treatment plants, as well as pesticide and fertilizer use associated with agriculture expansion (Luoma et al., 1998; Monroe & Kelly, 1992).

The European-period increase in urbanization and industrialization has led to the buildup of heavy metal contamination and a decrease in water quality in the San Francisco Bay watershed (Ritson et al., 1999, Luoma et al., 1998; Hornberger et al., 1999). Heavy metal contaminants, (Ag, Cu, Cr, Pb, Ni, Se, Zn), considered toxic chemicals by the San Francisco Bay

Regional Monitoring Program (RMP), record concentrations above ambient levels in the bay. Salt marshes are flat and poorly drained areas, subject to flooding, erosion, or alteration for land expansion (Williams et al., 1994). These coastal zones are often sinks for heavy metals, which are absorbed and trapped into the sediment as they accumulate (Zhang et al., 2013; Williams et al., 1994).

Impacts of increasing pollution levels are of major concern to the disruption of biodiversity and ecosystem resilience (Williams et al., 1994). Most heavy metals occur in low concentrations in natural environments, but human activity can cause increased release and concentration of these, through production and emission by industry and other activities. Research has shown that increased human activity, such as mining, can increase transport of dissolved ions and metals into watersheds due to acceleration of crustal exposure and rock weathering (Bertine & Goldberg, 1971). River transport of many metals (e.g., Cu, Pb, Zn) is greater than during preindustrial conditions (Martin and Meybeck, 1979). Lead, which is also associated with earlier automotive fuels, is a toxin of particular concern and its emissions have decreased in recent years due to regulations and decreased use of leaded fuels (Smith et al., 1987). In the last 170 years, 95% of the historic tidal wetlands in the bay have been destroyed due to diking and filling, and tidal marsh coverage has reduced to levels less than 4-8% of pre-1850 levels, due to European settlement, urbanization of lands, and levee construction on marsh areas (Josselyn, 1983; Luoma et al., 1998; Ritson et al., 1999). The current concentrations of these metals, the relationship of those concentrations to natural variability, and the effects of heavy metal pollutants on the biota of remaining marshes is yet another threat to marshes but is still not well understood (Bai et al, 2011; Williams et al 1994; Hornberger et al., 1999).

These sedimentological records of heavy metal contamination have been used to provide insight into the chronology of quantifiable levels of anthropogenic pollution (Zhang et al., 2013, Connor & Thomas, 2003; Hornberger et al., 1999, Valette-silver, 1993; Daskalakis & Connor, 1995; Williams et al., 1994; Ritson et al., 1999). However, the studies of long-term trends of heavy metal pollution in marshes are few and far between. Although there have been some studies that look at sediment cores from the San Francisco Bay itself, many of these studies do not look further back than the commencement of European settlement or over the past few centuries (Hornberger et al., 1999; Luoma et al., 1998; Ritson et al., 1999).

Understanding fluctuations in heavy metal concentrations in salt marsh sediments over long-term periods provides a more holistic view of heavy metal variability, the true impact of recent human activity relative to natural variability, and ecosystem resilience to periods of such disturbance. This study provides the longest and highest resolution heavy metal accumulation data from a San Francisco Bay marsh. In addition, the data is used to explore the relationship to the sedimentological and biological accretionary history, and geochemical changes, as a response to climatic and anthropogenic changes since the mid-Holocene. Our sedimentary core, taken from Petaluma marsh, and spanning the past approximately 6000 ± 170.5 YBP, provides detailed evidence of natural and anthropogenic changes in metal concentration and evidence of the resilience of the marsh to climatic and anthropogenic disturbance. Our research aims to better inform restoration ecologists and policy makers, specifically in terms of marsh dynamics and heavy-metal pollutants.

Figure 1 – (Left): Google Maps image of core extraction site in the Petaluma River Watershed. (Top): Google maps image close-up of vegetated marsh site. (Right): Picture of Petaluma marsh taken from a boat on the river.

Study Site

The San Francisco Bay is the largest estuary in western North America (Geen & Luoma 1998). The Petaluma Marsh Wildlife Area is the largest remaining salt marsh in the San Pablo Bay portion of the San Francisco Bay. The Petaluma River Watershed (Figure 1) is located in southern Sonoma County and northeastern Marin County. The watershed encompasses a 378-kilometer basin and is approximately 30 km long and 19 km wide. The city of Petaluma is centrally located within the watershed. Our study was conducted at the Petaluma marsh, which lies within the lower 32 km of the Petaluma River Watershed, extending into San Pablo Bay. The lower 19 km of the Petaluma river flow through the salt marsh. The marsh is surrounded by approximately 2833 Ha of reclaimed wetlands and is comprised of approximately 2023 Ha. There are creeks located on the eastern and western side of the watershed that drain into the Petaluma river and provide fresh water and sediment to the marsh areas. On the east side of the watershed there are Lichau Creek, Lunch, Creek, Adobe Creek, and Ellis Creek. On the western side there are Weigand's Creek, Marin Creek, and San Antonio Creek.

The San Francisco Bay region is characterized as having a Mediterranean climate, with a cool rainy season from late October to mid-April, in which 94% of the annual precipitation falls

(Josselyn, 1983), and a dry season from May through September characterized by little to no precipitation and cool marine air along the coast and hotter, dry weather inland. Precipitation highly influences the flow rates of the Petaluma river, which can experience from 50 to 127 cm of annual rainfall at the highest elevations of the drainage basin (SSCRCD 1999). This can affect the salinity of the marsh and associated soils, which can be very saline during the dry season, and closer to fresh water marshes conditions during the rainy season. Average annual temperature in the is 14.3° C, with a range from 7.1° C to 21.4° C (SSCRCD 1999).

The Petaluma River Basin lies within the northern Coast Ranges of California. The Franciscan complex, the oldest geologic unit in the study area (Jurassic and Cretaceous age), comprises the basement rock of the watershed. On top of the basement rock are deposits from the Tertiary and Quaternary. From the mid-to-late Pliocene, folding and faulting occurred within the basin and created the Petaluma formation which is present today. Prior to sea level rise, 10,000-11,000 years ago, the surficial deposits of the valley were comprised of sands, gravels, and clays deposited by streams. During this time sea level rose, approximately 60 m, and filled the lower portion of the valley with soft marine silts, consolidated clay and shale with minor amounts of sandstone (Josselyn, 1983). As sea level rise slowed, approximately 7,000 to 6,000 years ago, seawater began to flow into the south bay and the Suisun Basin, bringing with it sediment that allowed the bay to expand at a rate faster than sea-level rise (Josselyn, 1983). This allowed room for tidal wetland establishment, and bayward growth of marshes.

Post-European settlement human impacts have also affected the extent of coastal salt marshes. In the San Francisco Bay, historic development and expansion of some marsh habitat have been linked to large amounts of sediment being delivered from land clearing, hydraulic mining debris, and agriculture practices such as introduction of livestock (Atwater, 1979;

Hilgartner et al., 2006; Watson et al., 2013). This, in some cases, led to increased shallow water areas and marsh expansion.

Vegetation at Petaluma marsh follows the typical northern California salt marsh plant assemblages. The salinity gradient within the marsh affects the wetland vegetation, with salt marsh plants dominating specific areas. Discharge of freshwater into the San Francisco Bay and the Petaluma Marsh is highest in winter and early spring, owing to direct runoff and snowmelt in the case of the Bay. This influences the salinity of the Bay, with average salinities declining to 25 ppt (Josselyn, 1983). The two main halophytic plants that dominate the Petaluma salt marsh community are Pacific cordgrass (Spartina foliosa) and perennial pickleweed (Salicornia pacifica, formerly virginica). Pacific cordgrass is found at lower, intertidal elevations, while pickleweed is found at higher elevations. Some less dominant species that are present at the salt marsh are Alkali heath (Frankenia grandifolia), Saltgrass (Distichlis spicata), and Bulrush (Schoenoplectus spp.), with the ladder being found in more freshwater regions. The Petaluma River Watershed contains endangered flora at the marsh, including soft bird's-beak (Cordylanthus mollis ssp. mollis), showy Indian clover (Trifolium amoenum), and Sebastopol meadowfoam (Limnanthes vinculans). There are many channels running through the marsh plane, which can increase the distribution of tidal flooding with a marsh. Previous research done at Petaluma marsh has shown the influence of tidal channel size and distribution on increased species richness in vegetation along channel banks, as well as proximity to tidal channel networks (Sanderson et al., 2000; 2001).

Historical Land Use

Petaluma, originally called Péta Lúuma by the Coast Miwok inhabitants, came into the possession of Mariano Guadalupe Vallejo in 1834 through a Mexican land grant. During the late

1840s, American settlers came to Petaluma as part of the migration based on exploiting gold deposits that were being found in the Sierra Nevada (Ritson et al., 1999). Following this expansion in population came an expansion in agriculture and industrialization in the coastal region (Josselyn, 1983; Luoma et al., 1998). From 1860 to 1910, the estuaries were used for agricultural purposes to provide land for grazing, as well as cereal grains and row crops (Josselyn, 1983). As existing tidal marshes were being lost due to diking and conversion, other marshes were being created through sedimentation, largely coming from hydraulic mining for gold (Josselyn, 1983).

In addition to substantial amounts of sediment being released into streams and rivers, and eventually into the estuaries, through hydraulic gold mining, runoff from the urban watershed and fresh water inputs from municipal wastewater treatment plants were also delivering nutrients and contaminants, such as heavy metals (Ritson et al., 1999; Luoma et al., 1998; Hwang et al., 2006). During this late 1800s and early 1900s expansion, lead contamination increased in the estuaries through inputs from the Selby lead smelter facility near San Pablo Bay, and through the introduction of leaded gasoline in 1923 (Ritson et al., 1999). Contemporary inputs of heavy metal contamination are dominantly through anthropogenic inputs, such as runoff from urban centers, municipal plants, and atmospheric deposition, (Ritson et al., 1999; Monroe & Kelly, 1992; Walker, 2001). Lead input in particular from anthropogenic sources still accounts for more than 50% of total lead load in the San Francisco Bay, with lead persistence levels of decades found in the San Francisco estuary system (Hwang et al, 2006).

Methods

Field methods

To reconstruct the history of marsh establishment in Petaluma marsh, a 12-meter-long sediment core was collected. The salt marsh core extraction site is located at 38.167° N, and 122.551° W. The first 8 meters of the sediment core were collected in July, summer of 2015. The remaining 4 meters of the sediment core used in this study were collected in June, summer of 2016. The individual core location can be seen in Figure 1. The core depth totaled 12 meters. Samples were wrapped in the field and stored in a cold room at 4°C at the MacDonald Biogeography Laboratory at UCLA.

Lab methods

Cores were laid out in the lab and photos were taken to assess changes in color and lithology based on Munsell's Sediment Color Charts. Magnetic susceptibility was taken at 1cm intervals throughout the twelve-meter core using the Bartington MS3 magnetic susceptibility device and software (Thompson & Battarbee, 1975). The core was sliced into one-centimeter intervals, wrapped and stored in a cold room at 4°C. From each slice, a 1 cubic centimeter sample was extracted, dehydrated overnight, burned at 550°C for 4 hours, and at 950°C for 1 hour in order to measure the water content as a percentage of wet weight, bulk density in grams per cubic centimeter, organic content as a percentage of bulk density, and carbonate content as a percentage of bulk density, following the guidelines of Heiri, Lotter, & Lemcke, 2001 [Table 1].

Table 1 – *Formulas for LOI % Content Calculations*

% Water Content	$\frac{WW - DW}{WW} \; x \; 100$	DW = dry weight WW = wet weight LOI_1 = weight post 550°C LOI_2 = weight post 950°C
Bulk Density	$\frac{DW}{1 \; cc}$	
% Organic Matter	$\frac{DW - LOI_1}{DW} \; x \; 100$	
% Carbonate Content	$\frac{LOI_1 - LOI_2}{DW} \; x \; 100$	

Dating techniques

Macrofossil samples for radiocarbon dating were taken from varying depths along the core. The core was assessed at each centimeter for aboveground plant matter.

Organic samples chosen were located horizontally in the sediment. Nine samples from core PTL 15-02 and PTL 16-02 were used for AMS 14C measurements. A marine shell sample from core PTL 16-02 at basal depth 1123-1124 was used due to lack of other datable materials such as organic material. Samples were picked with tweezers and sieved to remove silt, clay, and other materials. Samples were dehydrated and placed in a glass bottle for storage.

Radiocarbon dating was conducted at the UC Irvine Keck Radiocarbon lab using a 500 kV compact AMS (accelerator mass spectrometer) unit from National Electrostatics Corporation. Macrofossil samples were pretreated with an acid-base-acid wash to remove any modern residues on the samples. Samples were placed in a glass tub with cobalt powder, sealed, combusted, and then graphitized. Carbonate samples were pretreated following the leaching and hydrolysis protocol, and then graphitized following KCCAMS/UCI facilities hydrogen reduction method (Santos, Moore, & Southon, 2007). THE UCI AMS results were calibrated using CALIB Radiocarbon Calibration (Stuiver et al., 2018). Marine shells were calibrated with the Marine09 calibration curve while organics were calibrated using the IntCal09 terrestrial calibration curve (Reimer et al., 2011). A Bayesian age-depth model was developed through BACON 2.2 (Blaauw and Christen, 2013), a software using R interface.

Using a conservative estimate of approximately 3 - 6 mm yr^{-1} of sediment accretion (Lauren Brown, personal communication), we estimated the year 1963 ^{137}Cs bomb spike would be at approximately 15 – 30 cm depth in the core. A 2-4 cm^3 sample was extracted approximately every 2-4 cm to 40 cm depth in core PTL15-02. This sampling strategy was used to ensure adequate sampling of the perspective ^{137}Cs peak as well as adequate resolution for the ^{210}Pb decay curve. After samples were extracted, they were dehydrated in a drying oven at 110°C for 24 hours and then weighed to calculate bulk density (g/cm^3). Then samples were ground,

sealed in plastic tubes, and sent to Doug Hammond's laboratory at USC where they were tested using a gamma counter for ^{137}Cs and ^{210}Pb activity. The ^{210}Pb and ^{137}Cesium curve is shown in [Figure 2].

XRF and statistical methods

To save on time and prevent destruction of the sample, a portable X-Ray Fluorescence (pXRF) machine was used to obtain elemental concentrations as opposed to wet chemistry elemental analysis techniques, such as acid washes that take several hours and additional resources for preparation. Although normalization calibrations were used to standardize the data set, sample concentrations may appear lower than current concentrations because of the presence of water in the soil.

A handheld, battery operated Innov-x Model 2000 XRF Analyzer was used on the entirety of the core at 2-3cm intervals to detect and quantify elemental compositions, including Ti, Cr, Mn, Fe, Ni, Cu, Zn, As, Se, Rb, Sr, Zr, Mo, Ag, Cd, Sb, Ba, Hg, Sn, and Pb. The concentration of elements measured by the instrument range from parts-per-million (ppm) to 100% by weight (XRF Manual). The Compton Normalization method calibration was used to normalize the data. Sample moisture can affect XRF results. However, the Compton Normalization method implemented automatically corrects results for these changes to the soil matrix. This creates more accurate dry weight results for the soil samples, which can then be compared to Laboratory dry weight results (XRF Manual).

The zonation of the chemical stratigraphy was based on cluster analysis and dendrograms and was created using the Rioja package software version 0.9-15 (Juggins, 2017) in the R Studio interface, as well as the Vegan package version 2.4-6 (Oksanen et al., 2018) in R. The Euclidean Dissimilarity Index was the metric distance measure chosen for cluster analysis due to the

continuous nature of our dataset. A broken stick model within the Vegan software was used to determine the optimal number of groups for zonation of the data. A constrained hierarchical clustering of the distance matrix was used, using the default agglomeration method CONISS.

Principal Component Analysis (PCA) is useful statistical method when looking at multivariate data for reducing the number of dimensions in a dataset by extracting the principal orthogonal components of the data. PCA has been used within the environmental sciences as a way to explore the primary drivers behind multivariate environmental processes (Mackenzie et al., 2017; Margalef et al., 2013; Monjerezi et al., 2011; Muller et al., 2008). PCA was run using the Vegan package software in R interface. PCA was run to extract the main components of variability of the geochemical data (i.e., Organics, Carbonates, Magnetic Sus., XRF) after standardizing and omitting rows with missing values. PCA has successfully been used within geochemical research to extract combinations of variables and explore the relationships within sites (Petterson et al., 1993; Rose & Juggins, 1994; Kähkönen et al., 1997; Kirby et al., 2013). Although the combination of XRF and PCA have mainly been used to look at lake sediments, recent research is advancing towards wetland sedimentary analysis (Margalef et al., 2013; Huang et al., 2017; Mackenzie et al., 2017). To further understand the significant of the relationships between the elements and their relationships to organic and carbonate content, a correlation matrix was run on the data. The correlation matrix was computed using the Hmisc and Corrplot packages in R Studio interface.

Results

Chronology

The uncalibrated and calibrated results from ^{14}C dating of 9 samples appears in Table 2. The stratigraphy and ^{14}C dating results of core PTL 15-02 and PTL 16-02 are displayed in Figure 3. Core PTL 15-02 and 16-02 consisted of 4 sediment types [Figure 3].

The oldest sediments at Petaluma River Estuary date to 6000 ± 170 YBP from a marine shell date. With the exception of the few anomalously young dates, dating results show a chronological sequence in the temporal record. An age-depth model was calculated using the statistical modeling software Bacon 2.2 (Blaauw & Christen, 2011).

Among the nine samples dated for AMS ^{14}C at UCI Keck Radiocarbon lab, three anomalously young dates (PTL16-02_1107, PTL16-02 1170, and PTL16-02_1193) were rejected due to extreme stratigraphic reversal (Table 2). For the two pairs of dates at 1170cm and 1193cm, the stick material yielded much younger dates than the surrounding organic material that was dated. We suspect that the materials dated (both highly preserved sticks) were younger, intrusive organic material that contaminated the sediment during the retrieval process in the field.

Table 2 – Radiocarbon Results and Calibrated Ages

Petaluma River Watershed	**UCIAMS #**	**Depth (cm)**	**Material**	**δ14C**	**14C Age**	**±**	**Cal. Age Range (YBP)**	**Mean Cal. Age (YBP)**
PTL15-02	183277	223	Organics	-185.3	1645	15	1525 - 1569	1547 ± 22
PTL15-02	183278	411	Organics	-257.4	2390	30	2346 - 2491	2418.5 ±72.5
PTL15-02	183279	652	Organics	-384.4	3895	25	4280 - 4415	4347.5 ± 67.5
PTL16-02	160407	799	Organics	-433.7	4570	20	5136 - 5319	5227.5 ± 91.5
PTL16-02	191919	988	Organics	-442.5	4695	15	5325 - 5470	5397.5 ± 72.5
PTL16-02	191918	1107	Stick	-15.8	130	15	-	-
PTL16-02	185583	1124	Shell	-520.2	5900	15	5829 - 6170	5999.5 ± 170.5
PTL16-02	183280	1170	Organics	40.3	-310	15	-	-
PTL16-03	191916	1193	Stick	86.2	Modern		-	-

Accretion Rates

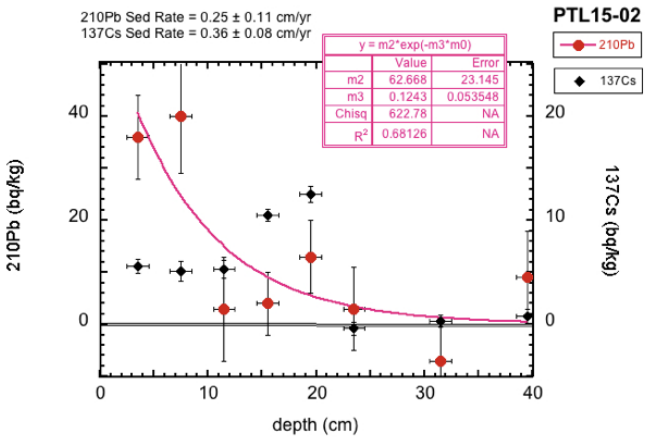

Figure 2 – Pb-210 and Cesium curve accretion rates for Petaluma marsh, conducted at USC done by Doug Hammond.

The ^{210}Pb and ^{137}Cesium curve is shown in Figure 2. Based on an estimated 1963 ^{137}Cs peak being 20 cm depth (± 2 years), the average accretion at Petaluma Marsh is 3.6 mm yr^{-1} ± 0.8. Using a constant rate of supply (CRS) model which assumes of a constant supply of unsupported radioactive ^{210}Pb to the marsh surface and then uses the radioactive decay rate as a temporal control (Appleby & Oldfield, 1978), the estimation of accretion given by ^{210}Pb is 2.5 mm yr^{-1} ± 0.11, which is 1 mm less than the accretion rate estimated by ^{137}Cs. This disagreement between ^{210}Pb and ^{137}Cs accretion rates is not unexpected, as accretion may be different over different time periods, and this could reflect that variation in rates. It is important to note however that there is some variability in the ^{210}Pb activity (for instance at 12 cm and 32 cm depth) that could indicate bioturbation of the sediments, disturbing the record.

Stratigraphy and environmental changes

The upper 10 cm of the Petaluma core are composed of highly organic sediment overlying a layer of peat-like, organic marsh sediment, seen in Figure 3. This peaty layer extends from about 10 cm to 250 cm. From 300 cm to 750 cm there are combinations of silty peat, silty clay, with brown or black striations throughout [see Figure 3]. The lower mid-to-basal depths of the core, around 800 cm to 1100 cm, are represented by watery, silt and clay layers, interspersed with small layers of highly organic material. The basal meter layer, 1100 cm to1200 cm, is

characterized by silty clay, with no presence of black or brown striations typical of overlying organics and is interspersed with marine shells. The core terminates in coarse-grained, basal marine or fluvial sediments.

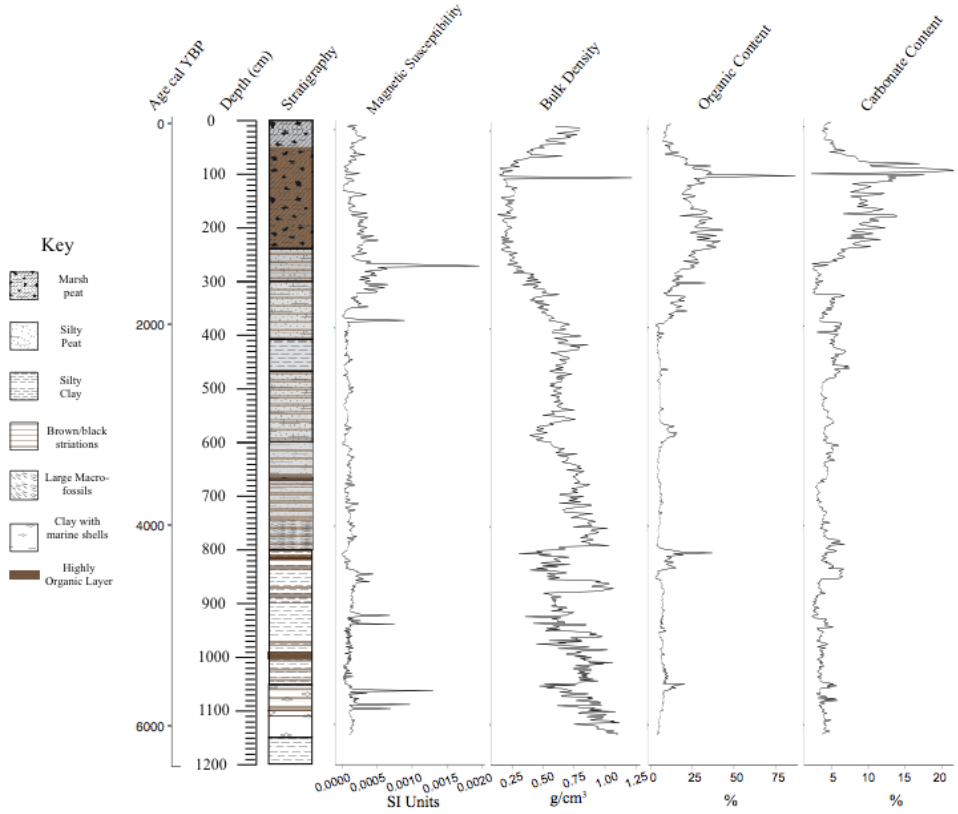

Figure 3 - Stratigraphic diagram of core PTL 15-02 and PTL 16-02 from Petaluma marsh. Core has a basal date of 6109 YPB. Color, texture, and macrofossil content as well as changes in organic and carbonate content indicate that marsh first appeared at this site around 300 cm in depth, an estimated 1970 YBP. Sediments below the marsh interface range from silty peat to silty clay, ending with silty clay, possibly indicative of an intertidal channel being present before the marsh began to form.

The Petaluma core was subjected to magnetic susceptibility testing and centimeter-resolution LOI. The stratigraphy diagrams appear in Fig. 3. Highest susceptibility is found in the upper core. The core shows a large increase and then decrease in organic content towards the top, around 50 to 350 cm, which reflects the establishment of the marsh and the subsequent increased organic deposition of organics, particularly of plant material. There is a peak at 75 cm depth; 471 YBP. The increases in carbonate content seem to occur not long after the increases in organic material, ranging from 50 cm to 250 cm, with a period of increased carbonate content around 75

cm to 125 cm. Both organic and carbonate percent content decrease from 50 cm to modern conditions at the marsh. Bulk density also increases during this period, starting from 60 cm, or 358 cal YBP, to modern times. Organic content decreases below the period of marsh establishment, around 350 cm depth, with intermittent period of increased content around 550 cm, 800 to 835 cm, and 1050 cm depths. Carbonate content shows relative consistency between 3 and 7 percent concentrations, which provide evidence for intertidal mudflats being present prior to the establishment of the salt marsh. Marine shells, which are found around 1050 to 1200 cm depths, have increased levels of carbonate and can be a likely contributor to these signals. Shifts seen in the magnetic susceptibility diagram [Figure 3] are likely indicative of changes in sediment source and content (Thompson & Battarbee, 1975). The highest peak in the magnetic susceptibility begins around 370 cm depth, which is similar to the period of time in which the organic content in the marsh begins to increase.

XRF Analysis

This research used two datasets in the multivariate statistical analysis of elemental components and bulk density, organic carbonate, and carbonate content. The first dataset consists of heavy metal elements Cr, Mn, Fe, Ni, Cu, Zn, Rb, Sr, Zr, Ag, Ba and Pb. The second dataset consists of toxic heavy metal elements Cu, Cr, Ni, Zn, Pb, Se, and Ag. These elements were chosen based on the findings of Trowbridge et al., 2016 on the updated ambient concentrations of toxic chemicals in San Francisco Bay area sediments recorded from the regional monitoring program in San Francisco.

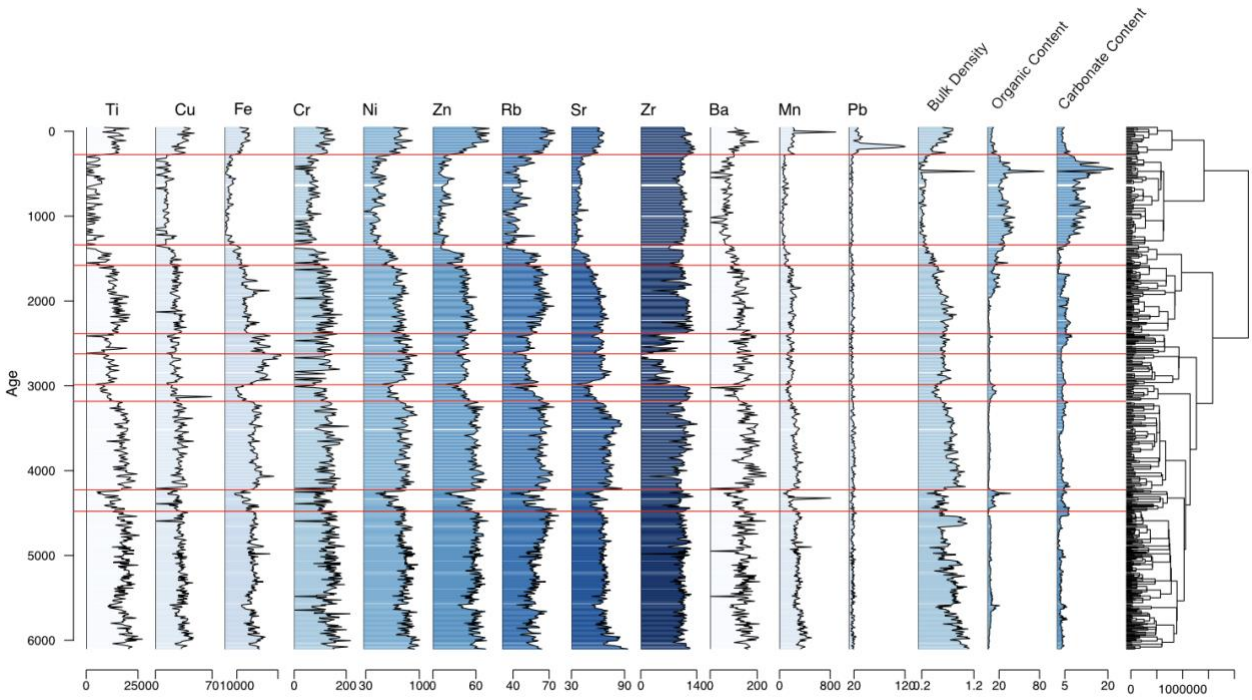

Figure 4 – Vertical distributions of heavy metals, bulk density, organic content and carbonate content for core Petaluma core. Rioja package in R used for zonation, cluster analysis, and dendrogram. Age is given in Cal Years BP from the BACON model. 10 zones are represented.

Vertical distributions of heavy metal elemental concentrations (Cr, Mn, Fe, Ni, Cu, Zn, Rb, Sr, Zr, Ag, Ba and Pb) are plotted in Figure 4 as absolute concentrations in parts per million (ppm). The concentrations of many of these elements in the deepest parts of the core represent areas without anthropogenic contamination via European industry and land-use practices. There are variations in the concentrations of many of the elements from 350 cm to 1200 cm depths. In the upper layers, around 200 cm to 50 cm, there is a decrease in heavy metals. In the most modern zone, from around 50 cm to modern marsh environments, concentrations of heavy metals begin to increase. The vertical profiles of the heavy metals reflect the historical effects of climatic sedimentological and anthropogenic influences on the sediment loadings of the Petaluma River watershed.

The dendrogram, zonation, and cluster analysis in Figure 4 and 7 was used to subdivide the XRF geochemical stratigraphy into discrete zones in order to examine the stratigraphy and

relationships between the elements, as well as the overall relationships between the elements and the organic and carbonate concentrations in the marsh. The optimal number of zones are 10, as suggested by the broken-stick model applied.

XRF data [Figure 4] show that the elemental concentrations vary significantly down the core. Importantly, the concentrations of Ti, Cu, Fe, Cr, Ni, Zn, Rb, Sr, Zr, Ba, Mn, in Zone 1 (44-0 cm; 252 cal yr BP-present) are not unprecedented within the core. Equally high concentrations for these elements are apparent in the parts of the pre-European era. The exception to this is Pb, which is much higher in Zone 1 than in other portions of the core. Zone 1 shows an increase in all elements and bulk density following the previous zone 2, and a decrease in organic and carbonate content. Zone 2(193-44 cm; 1318-252 cal yr BP) is dominated by the lowest values of most heavy metal elements, with the exception of Zr and Pb, and in bulk density, and the highest concentrations in organic and carbonate content. There is a peak of concentrations in bulk density and organic content, coupled with a substantial decrease in carbonate content at 75 cm depth, 471 cal yr BP. Zone 3(229-193 cm; 1562-1318 cal yr BP) shows a slight increase in elements Ti, Cu, Fe, Cr, Ni, Zn, Rb, Sr, Ba, Mn, and bulk density, with minimal change in elements Pb, Zn, and a decrease in organic and carbonate content. Zone 4(371-229 cm; 2367-1318 cal yr BP) shows a continued increase in elements Ti, Cu, Fe, Cr, Ni, Zn, Rb, Sr, Ba, Mn, bulk density, and carbonate content, with minimal change in elements Pb, Zn, and a decrease in organic content. Zone 5(413-371 cm; 2603-2367 cal yr BP) shows an increase in elements Fe, Ni, and Ba, with minimal change in elements Cr, Sr, Mn, Pb, bulk density and organic content, and a decrease in Ti, Cu, Zn, Rb, Zr, and carbonate content. Zone 6(467-413 cm; 2967-2603 cal yr BP) shows slight to moderate increases in elements Ti, Fe, Cr, Ni, Sr, Ba, minimal change in elements Cu, Zr, Rb, Mn, Pb, bulk density, organic content and carbonate content, and a decrease

in elements Zn. Zone 7(495-467 cm; 3156-2967 cal yr BP) shows a dip followed by increased concentrations in elements Ti, Cu, Fe, Cr, Ni, Zn, Rb, Sr, Ba, Mn, bulk density, and carbonate content, minimal changes in Pb, and an increase in Zr and organic content. Zone 8(653-495 cm; 4211-3156 cal yr BP) shows increased and maintained concentrations throughout for elements Ti, Cu, Fe, Cr, Ni, Zn, Rb, Sr, Zr, Ba, Mn, bulk density and carbonate content, with minimal change in Pb, organic content. Following zone 8 we see a dip in elemental concentrations, followed by an increase in Zone 9(707-653 cm; 4465-4211 cal yr BP) for elements Ti, Cu, Fe, Cr, Ni, Zn, Rb, Sr, Zr, Ba, bulk density and carbonate content, with a large spike in Mn similar to zone 1, and a small peak in organic content. Zone 10(1122-707 cm; 6103-4465 cal yr BP) represents moderated concentrations with the elements Ti, Cu, Fe, Cr, Ni, Zn, Sr, Zr, Ba, Mn, Pb, organic content and carbonate content, and a high increase at the beginning of the zone for Rb and bulk density.

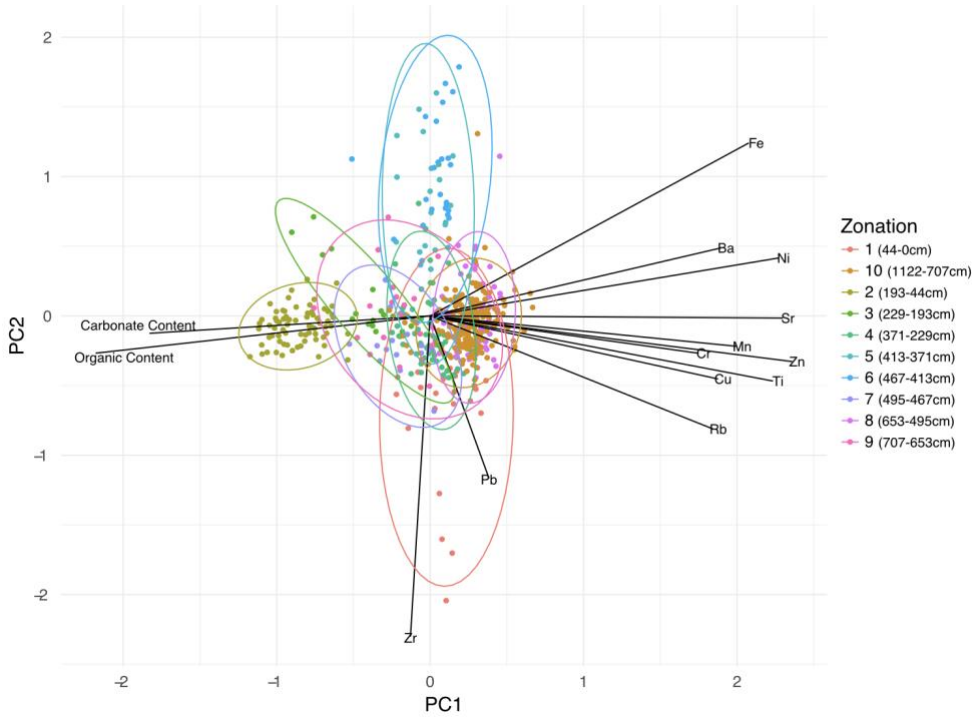

Figure 5 – Principle component analysis of XRF heavy metal elements, organic content and carbonate content by depth. Data were analyzed and graphed in RStudio (RStudio Team, 2015). The two axes explain 99.9% of the variance in the Petaluma core.

In this research PCA was used to reduce the dimensionality of the data in order to explore temporal trends within the elemental dataset and the organic and carbonate content within the core. The first axis presented in Figure 5 explains 99.6% of the variance, and the second axis explains 0.3%. As might be expected, there is a relationship between clustering of samples on the PCA ordination and the stratigraphic zonation of the elements down core. The PCA clustering of samples in Zone 2 is the most distinct from the rest of the zones. Zone 5 and 6 are largely overlapping, with little overlapping in Zone 3 and Zone 9. Zone 1 partly overlaps with Zone 7, Zone 8, and Zone 9, with the majority of overlap found in Zone 10.

A negative relationship between the elements and organic and carbonate content is suggested by the PCA plot [Figure 5], where the concentrations of heavy metals are concentrated on the right of the plot, while the organic and carbonate content are concentrated on the left-hand side. All heavy metal elements, with the exception of Zr, have positive loadings on the first component, while Zr, organic and carbonate content have negative loadings. Sr, Mn, Cr, Zn, Ti, Cu, Rb, Pb, Zr, organic content, and carbonate content have negative loadings on the second principal component, while Fe, Ba, and Ni have positive loadings. Mn, Cr, Zn, Ti, and Cu are strongly correlated in this site [Figure 6] and show an inverse relationship with organic and carbonate content within the core. Zr shows little influence from organic and carbonate content. Pb also exhibits more influence than Zr, but less of an influence from organic and carbonate content compared to elements Mn, Cr, Zn, Ti, and Cu. The elements Fe, Ba, Ni, and Sr also ordinate opposite to organic and carbonate content.

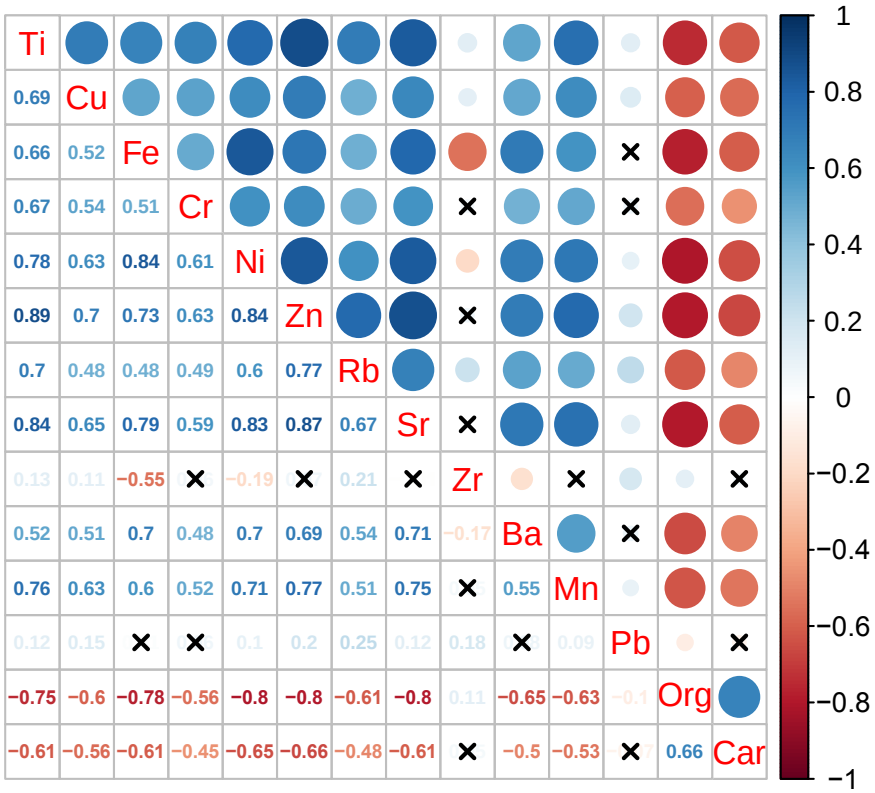

Figure 6 – A table with R values and significant values of correlation coefficients calculated between all the heavy metal elements and organic and carbonate content. The numerical values represent correlation coefficients (R values), and the crosses refer to insignificant correlations (P < 0.05). The color intensity and circle sizes both indicate the magnitudes of the R values.

Figure 6 presents the significance of the relationships between heavy metals and their relation to organic and carbonate content in a correlation matrix. There are significant negative correlations between organic content and the heavy metals, with the exception of Zr, which has a slightly positive correlation coefficient of 0.11. The negative correlations between the heavy metals and organic content suggest that there is no bioaccumulation occurring within this site.

With the exception of Pb and Zr, the metals are significantly positively correlated with each other, and negatively correlated with carbonate content. This presumably reflects that the heavy metals are present in the bedrock and inorganic sediments of the terrestrial watershed and are mainly arriving due to natural erosion and deposition prior to European arrival and the increased erosion of the watershed post-European arrival due to the introduction of ranching, farming, and urban development. Zr is known to be abundant and naturally occurring, although

there has been research that shows atmospheric increases due to industry and nuclear weapons (Shahid et al., 2013). Zr has also been found to be toxic to plants and plays a role in reducing plant growth (Shahid et al., 2013). However, the slightly positive correlation between Zr and organic content, as well as the limited variability between Zr concentrations and organic content increase [Figure 4] suggest that this is not the case at this site. Pb has a weak significant correlation with some metals – and this, coupled with the high concentration values of Pb during the European periods, indicates that in pre-European times only small amounts of lead were coming in with other heavy metals in the watershed sediment. In addition, the high peak at the top of the core is related to human activity that created unprecedented levels of Pb.

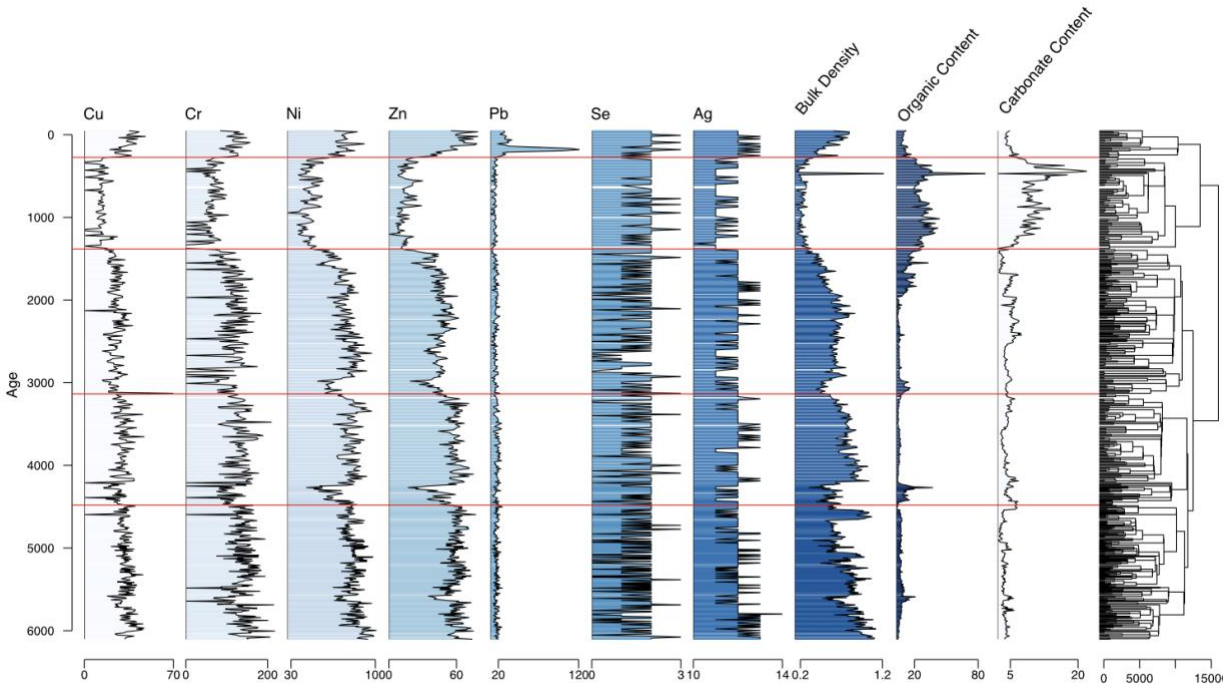

Figure 7 – Vertical distributions of toxic heavy metals, bulk density, organic content and carbonate content for core Petaluma core. Rioja package in R used for zonation, cluster analysis, and dendrogram. Age is given in Cal Years BP from the BACON model. 10 zones represented.

Vertical distributions of toxic heavy metal elemental concentrations (Cu, Cr, Ni, Zn, Pb, Se, and Ag) are plotted in Figure 7 as absolute concentrations in parts per million (ppm). The

optimal number of zones for the toxic heavy elements are the organic and carbonate contents of the marsh are 5, as suggested by the broken-stick model in the Vegan package in the R interface.

To explore the toxic heavy metals in detail a separate PCA was run on the XRF data [Figure 8]. The stratigraphy again shows that the elemental concentrations of Cu, Cr, Ni, Zn, and Ag in Zone 1(44-0 cm; 252 cal yr BP-present) are not unprecedented within the core. The exception to this is Pb. Se resolution is poor but may have its highest centrations in this zone. Zone 1 shows an increase in all elements and bulk density following the previous zone 2, and a decrease in organic and carbonate content. Zone 2(197-44 cm; 1347-252 cal yr BP) is dominated by the lowest values of all heavy metal elements and bulk density, with the exception of Se and Pb, and the highest concentrations in organic and carbonate content. The peak is seen here with regards to concentrations of bulk density and organic content, coupled with a substantial decrease in carbonate content at 75 cm depth, 471 cal yr BP. Zone 3(489-197 cm; 3116-1347 cal yr BP) shows variable increases in elements Cu, Cr, Ni, Zn, Se, Ag, and bulk density, organic content and carbonate content, with minimal change in elements Pb, Se. Zone 4(707-489 cm; 4465-3116 cal yr BP) shows continued variable increases in elements Cu, Cr, Ni, Zn, Se, Ag, and bulk density, organic content and carbonate content, with minimal change in elements Pb, Se, Ag. Zone 5(1122-707 cm; 6103-4465 cal yr BP) represents moderated concentrations with the elements Cu, Cr, Ni, Zn, Pb, Se, Ag, organic content and carbonate content, and a high increase at the beginning of the zone for bulk density.

PCA was run on toxic heavy metals in addition to explore trends in elemental composition and the relationship with organic and carbonate content within the core. A very similar inverse relationship between the toxic heavy metals and organic and carbonate content is presented in Figure 8. The first axis explains 82.48% of the variance, and the second axis

explains 11.03% in the Petaluma core. Similar to the heavy metal PCA plot, Zone 2 is the most distinct from the rest of the zones in the dataset, while Zone 1 partly overlaps with Zone 3, and Zone 4, with complete overlap found in Zone 5.

Differences between the elements and organic and carbonate content are clearly represented in the PCA plot [Figure 8], with the exception is Pb and Se, where the concentrations of heavy metals ordinate on the left of the plot, while the organic and carbonate content are concentrated on the right-hand side. All toxic heavy metals, with the exception of Se, contributed negatively to the first component, while Se, organic and carbonate content positively contributed [Figure 6]. Se, Pb, Ag, Cu, Zn, Cr, organic content, and carbonate content positively contributed to the second principal component, while Ni negatively contributed. Zn and Cr show an inverse relationship with organic and carbonate content within the core. Pb shows little influence from organic and carbonate content, while Zr appears to be slightly influenced by them. Ni shows an inverse relationship with carbonate content, as well as organic content. The elements Cu and Ag also ordinate opposite to organic and carbonate content, with Ag showing less influence.

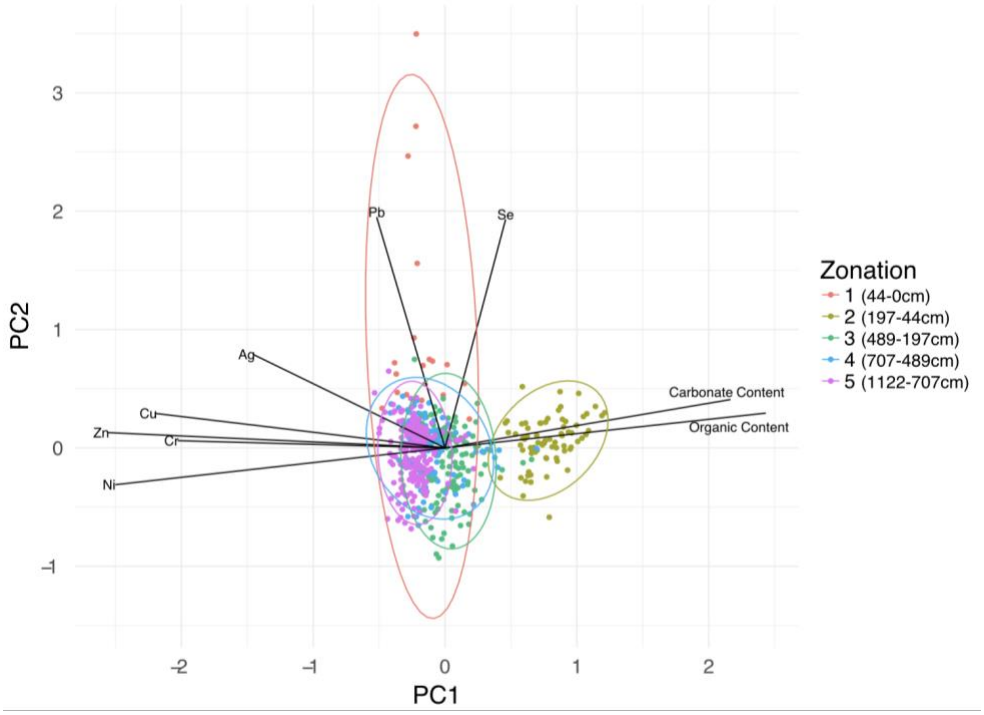

Figure 8 – Principle component analysis of XRF toxic heavy metal elements, organic content and carbonate content by depth. Data were analyzed and graphed in RStudio (RStudio Team, 2015). The first two axes explain 93.5% of the variance in the Petaluma core.

Discussion

The sediments and radiocarbon dates from the Petaluma core show that the upper salt marsh ecosystem, as represented by the high organic and fibrous material in the upper portion of the core is a geologically recent development. Bayesian-age depth modeling of the stratigraphy shows that high levels of organics in silty and marshy peat are interspersed throughout the core, around 1000cm or 5573 YBP, 820cm or 4918 YBP, and 670cm or 4239 YBP, but did not lead to marsh establishment until after around 350 cm, or around 1900 YBP [Figure 3]. Prior to the establishment of marsh vegetation expansion, the ecosystem most likely resembled a tidal flat with low marsh components or nearby low marsh. This is consistent with similar studies looking at marsh expansion in the San Francisco Bay area (Byrne et al., 1988; Wells et al., 1997) which concluded that marshes at China camp and Peyton Hill were established around 2000 YBP and

3000 YBP. The estimated date of marsh establishment is preliminary in nature, and a higher resolution of radiocarbon dating around 350-450 cm would provide a more precise estimate.

The average rate of accretion at Petaluma Marsh is 3.6 mm yr -1 ± 0.8. As stated previously, the estimation of accretion given by ^{210}Pb is 2.5 mm yr^{-1} ± 0.11, which is 1 mm less than the accretion rate estimated by ^{137}Cs. This disagreement between ^{210}Pb and ^{137}Cs accretion rates is not unexpected, as accretion may be different over different time periods, and this could reflect that variation in rates. The variability in the ^{210}Pb activity possibly indicates bioturbation of the sediments, and a possible disturbance within the record. The core should undergo further chronological analysis, which will include more ^{137}Cs and ^{210}Pb dating for a more accurate understanding of marsh accretion in more recent years. This preliminary work coupled with future chronological dating will provide a more complete picture of the Petaluma marsh establishment and expansion in the watershed.

Increases in bulk density and decreases in organic and carbonate content in the more recent past, around 270 years ago based on the preliminary ^{14}C dating, are likely due to post-European settlement and anthropogenic influences, confirming anthropogenic impacts on the Petaluma watershed over the last 150-200 years following European arrival. Anthropogenic inputs come from sources such as the hydraulic mining in the 1850s, and the following urbanization of Petaluma city which led to increases in runoff from urban centers and highways, municipal plants, and atmospheric deposition of lead. These land use changes have impacts on the delivery rates of sediment to the marsh which can promote marsh development as well as inhibit marshland expansion (Gallagher, 1996; Kirwan et al., 2011). The decrease in organic and carbonate content from 50 cm depth, or 300 YBP, is likely a result of changes in sedimentation regimes likely relate to European colonization and subsequent urbanization (Gallagher, 1996;

Kirwan et al., 2011). The increase in bulk density during this period, starting from 60 cm, or 358 cal YBP, to modern times could be indicative of urbanization and land use changes leading to increased runoff, soil erosion and increased sedimentation in the watershed post-European settlement.

Magnetic susceptibility in the core shows increases around 5918-6090 YBP, 5300-5370 YBP, and 1686-2389 YBP. The highest peak in the magnetic susceptibility begins around the period of time in which the organic content in the marsh begins to increase, approximately 1798 YBP. This provides evidence for an event that lead to an increase in magnetics being retained in the sediment, which provided the ecosystem the opportunity for a vegetated marshland to establish. Thompson & Oldfield (1986) noted that the soil close to large towns and industrial centers can have a higher susceptibility than that elsewhere because magnetic spherules derived from burning coal are emitted into the atmosphere and fall onto the soil from it. The peaks in magnetics in the soil appear to follow and decrease in bulk density, possibly indicating a new sediment source (Thompson & Battarbee, 1975; Strzyszcz, Z., 1993).

The true vegetated Petaluma marsh ecosystem that is present began to develop around 1900 YBP, although there are a few periods of vegetated sediments interspersed throughout the core. With this formation of the marsh we see a decline in heavy metals derived from natural sources in the watershed. With the arrival of Europeans, erosion in the watershed led to decreased organics as eroded crustal material – including heavy metals – was deposited on the site. Industrial activity, and later gasoline containing lead, produced depositions of Pb concentrations higher than any time in the past, when largely only natural processes were at work.

The heavy metal concentration patterns in the Petaluma marsh sediment core show an enrichment in most elements in the core, specifically Ni, Zn, Rb, Zr, Mn, and Pb, in the upper 1-44cm. This increase can be due to increases in bulk sediment contents, such as clays or organic carbon contents, and from anthropogenic sources. Modern lead concentrations appear to be seven times greater than lead concentrations from a century ago (Chow et al., 1973; Bruland 1974). The high peak of Pb from 32-36cm, around 166-195 YBP, are most likely influenced by European land use following the Gold rush and leaded gasoline centers in the 1950s. Pb and Cr concentrations have been reported to be associated with anthropogenic origin (Meena et al., 2017). The reducing conditions in estuarine sediments naturally show large quantities of metals, such as iron, which provide the elements necessary for degradation of organic substances. Mn concentrations vary with the availability of oxygen in the peat, leaching under anaerobic conditions and becoming soluble and precipitating in aerobic conditions (Goldschmidt, 1958). The peak seen around 275cm, around 3654 YBP, most likely represents post-depositional diagenesis as the peat deposits become more anoxic (Muller et al., 2007). Iron is also affected by oxic and anoxic conditions, however Fe does not follow the pattern of Mn in Petaluma marsh.

Lithogenic elements, such as Ti, Pb, and Cu are related to mineral matter in peat deposits, and the results show an increase in these elemental concentrations as bulk density increases but organic inputs decrease. This can be due to soil erosion from diking, and runoff from urban centers. Copper is also known to be highly utilized by carbonate minerals and iron-manganese oxide minerals and is less mobile than lead and zinc (Prusty and others, 1994). Similarly, Ba has been seen as a source for carbonate substances in sediment soils, as well as an aid with sulfate-reducing bacteria in marsh environments (Nedwell & BBanat, 1981). Zn has some of the highest concentrations of heavy metal elements within the core. The major sources of Zn are from metal

production, waste incineration, fossil fuels and fertilizers (Councell et al., 2004; Hwang et al., 2006; Meena et al., 2017). Silver (Ni) inputs in the San Francisco Bay have been recorded to come mostly from industrialization (Brown and Luoma, 1995). Rb abundance has been used as a monitor for clay fractions in intertidal sediments, while Sr and Zr abundance has been related to detrital feldspar in silty and sandy fractions in the soil (Varekamp, J. C., 1991). Zr is known to be abundant and naturally occurring, with recent atmospheric increases due to industry and nuclear weapons (Shahid et al., 2013). The negative correlations between these heavy metals and organic content, which can be seen in the correlation matrix [Figure 6], suggest that there is no bioaccumulation occurring within this site.

Conclusions

Our multi-proxy record from the Petaluma watershed provides one of the oldest and longest paleo-geochemical records for the region. Evidence from long-term geochemical data in the Petaluma marsh, spanning the past 6100 years, shows that the current Petaluma marsh ecosystem was not well established until around 2000 YBP. The physical properties of the Petaluma core demonstrate a dynamic and variable record of change through time. The transition from silt or sand to marsh peat shows that the environment became favorable for marsh expansion pre-European contact, while the increases in inorganic sediment and bulk density towards the top of core show increased levels of sediment delivery to the marsh due to European colonization in Petaluma following the 1850s.

Our results also confirm that although there is an increase in many heavy metal and toxic heavy metal elements over the last 150-200 years due to post-European impacts on the watershed, with the exception of Pb and possibly Se, these concentrations are not unprecedented.

In addition, PCA analysis of the Petaluma core reveals a strong inverse relationship between organic and carbonate content and heavy metals in the sediment, with weaker relationships between Pb, Se, and Zr. In addition, or results show that there is a negative correlation between heavy metal elements and organic content in the marsh. This suggests there is no evidence of bioaccumulation in the site.

References

Appleby, P. G., & Oldfield, F. (1978). The calculation of lead-210 dates assuming a constant rate of supply of unsupported 210Pb to the sediment. Catena, 5(1), 1-8.

Atwater, B. F. (1979). Ancient processes at the site of Southern San Francisco Bay, movement of the crust and changes in sea level.

Bruland, K. W., Bertine, K., Koide, M., & Goldberg, E. D. (1974). History of metal pollution in southern California coastal zone. Environmental Science & Technology, 8(5), 425-432.

Bai, J., Xiao, R., Cui, B., Zhang, K., Wang, Q., Liu, X., ... & Huang, L. (2011). Assessment of heavy metal pollution in wetland soils from the young and old reclaimed regions in the Pearl River Estuary, South China. Environmental Pollution, 159(3), 817-824.

Bertine, K. K., & Goldberg, E. D. (1971). Fossil fuel combustion and the major sedimentary cycle. Science, 173(3993), 233-235.

Blaauw, M., & Christen, J. A. (2013). Bacon Manual e v2. 2. Blaauw, M., Wohlfarth, B., Christen, JA, Ampel, L., Veres, D., Hughen, KA, Preusser, F., et al.(2010),—Were Last Glacial Climate Events Simultaneous between Greenland and France, 387-394.

Connor, S. E., & Thomas, I. (2003). Sediments as archives of industrialisation: evidence of atmospheric pollution in coastal wetlands of southern Sydney, Australia. Water, Air, and Soil Pollution, 149(1-4), 189-210.

Brown, C. L., & Luoma, S. N. (1995). Use of the euryhaline bivalve Potamocorbula amurensis as a biosentinel species to assess trace metal contamination in San Francisco Bay. Marine Ecology Progress Series, 129-142.

Byrne, R., Ingram, B. L., Starratt, S., Malamud-Roam, F., Collins, J. N., & Conrad, M. E. (2001). Carbon-isotope, diatom, and pollen evidence for late Holocene salinity change in a brackish marsh in the San Francisco Estuary. Quaternary Research, 55(1), 66-76.

Councell, T. B., Duckenfield, K. U., Landa, E. R., & Callender, E. (2004). Tire-wear particles as a source of zinc to the environment. Environmental science & technology, 38(15), 4206-4214.

Daskalakis, K. D., & O'connor, T. P. (1995). Normalization and elemental sediment contamination in the coastal United States. Environmental Science & Technology, 29(2), 470-477.

Gallagher, J. (1996). Late Holocene evolution of the Chorro delta, Morro Bay, California. University of California, Los Angeles.

Gedan, K. B., Silliman, B. R., & Bertness, M. D. (2009). Centuries of human-driven change in salt marsh ecosystems.

Gilbert, G. K. (1917). Hydraulic-mining debris in the Sierra Nevada (No. 105). US Government Printing Office.

Goldschmidt V. M. (1958) Geochemistry. Oxford University Press, London.

Hilgartner, W. B., & Brush, G. S. (2006). Prehistoric habitat stability and post-settlement habitat change in a Chesapeake Bay freshwater tidal wetland, USA. The Holocene, 16(4), 479-494.

Hornberger, M. I., Luoma, S. N., van Geen, A., Fuller, C., & Anima, R. (1999). Historical trends of metals in the sediments of San Francisco Bay, California. Marine Chemistry, 64(1-2), 39-55.

Huang, J., Wan, S., Xiong, Z., Zhao, D., Liu, X., Li, A., & Li, T. (2016). Geochemical records of Taiwan-sourced sediments in the South China Sea linked to Holocene climate changes. Palaeogeography, Palaeoclimatology, Palaeoecology, 441, 871-881.

Hwang, H. M., Green, P. G., Higashi, R. M., & Young, T. M. (2006). Tidal salt marsh sediment in California, USA. Part 2: Occurrence and anthropogenic input of trace metals. Chemosphere, 64(11), 1899-1909.

Jari Oksanen, F. Guillaume Blanchet, Michael Friendly, Roeland Kindt, Pierre Legendre, Dan McGlinn, Peter R. Minchin, R. B. O'Hara, Gavin L. Simpson, Peter Solymos, M. Henry H. Stevens, Eduard Szoecs and Helene Wagner (2018). vegan: Community Ecology Package. R package version 2.4-6. https://CRAN.R-project.org/package=vegan

Josselyn, M. (1983). The ecology of San Francisco Bay tidal marshes: a community profile (No. FWS-/OBHS-83/23). SAN FRANCISCO STATE UNIV TIBURON CA TIBURON CENTER FOR ENVIRONMENTAL STUDIES.

Juggins, S. (2017) rioja: Analysis of Quaternary Science Data, R package version (0.9-15.1). (http://cran.r-project.org/package=rioja).

Kähkönen, M. A., Pantsar-Kallio, M., & Manninen, P. K. (1997). Analysing heavy metal concentrations in the different parts of Elodea canadensis and surface sediment with PCA in two boreal lakes in southern Finland. Chemosphere, 35(11), 2645-2656.

Kennish, M. J. (2001). Coastal salt marsh systems in the US: a review of anthropogenic impacts. Journal of Coastal Research, 731-748.

Kirby, M. E., Feakins, S. J., Bonuso, N., Fantozzi, J. M., & Hiner, C. A. (2013). Latest Pleistocene to Holocene hydroclimates from Lake Elsinore, California. Quaternary Science Reviews, 76, 1-15.

Kirwan, M. L., & Megonigal, J. P. (2013). Tidal wetland stability in the face of human impacts and sea-level rise. Nature, 504(7478), 53.

Kirwan, M. L., Murray, a. B., Donnelly, J. P., & Corbett, D. R. (2011). Rapid wetland expansion during European settlement and its implication for marsh survival under modern sediment delivery rates. Geology, 39(5), 507–510. doi:10.1130/G31789.1

Luoma, S. N., Van Geen, A., Lee, B. G., & Cloern, J. E. (1998). Metal uptake by phytoplankton during a bloom in South San Francisco Bay: Implications for metal cycling in estuaries. Limnology and Oceanography, 43(5), 1007-1016.

Mackenzie, L., Heijnis, H., Gadd, P., Moss, P., & Shulmeister, J. (2017). Geochemical investigation of the South Wellesley Island wetlands: Insight into wetland development during the Holocene in tropical northern Australia. The Holocene, 27(4), 566-578.

Margalef, O., Cañellas-Boltà, N., Pla-Rabes, S., Giralt, S., Pueyo, J. J., Joosten, H., ... & Moreno, A. (2013). A 70,000 year multiproxy record of climatic and environmental change from Rano Aroi peatland (Easter Island). Global and Planetary Change, 108, 72-84.

Martin, J. M., & Meybeck, M. (1979). Elemental mass-balance of material carried by major world rivers. Marine chemistry, 7(3), 173-206.

Meena, R. A. A., Sathishkumar, P., Ameen, F., Yusoff, A. R. M., & Gu, F. L. (2017). Heavy metal pollution in immobile and mobile components of lentic ecosystems—a review. Environmental Science and Pollution Research, 1-15.

Monjerezi, M., Vogt, R. D., Aagaard, P., & Saka, J. D. (2011). Hydro-geochemical processes in an area with saline groundwater in lower Shire River valley, Malawi: an integrated application of hierarchical cluster and principal component analyses. Applied Geochemistry, 26(8), 1399-1413.

Monroe, M. W., Kelly, J., & Lisowski, N. (1992). State of the Estuary. Report of the San Francisco Estuary Project. US Environmental Protection Agency, Oakland, California.

Muller, J., Kylander, M., Martinez-Cortizas, A., Wüst, R. A., Weiss, D., Blake, K., ... & Garcia-Sanchez, R. (2008). The use of principle component analyses in characterising trace and major elemental distribution in a 55 kyr peat deposit in tropical Australia: implications to paleoclimate. Geochimica et Cosmochimica Acta, 72(2), 449-463.

Nedwell, D. B., & Banat, I. M. (1981). Hydrogen as an electron donor for sulfate-reducing bacteria in slurries of salt marsh sediment. Microbial ecology, 7(4), 305-313.

Petterson, G., Renberg, I., Geladi, P., Lindberg, A., & Lindgren, F. (1993). Spatial uniformity of sediment accumulation in varved lake sediments in northern Sweden. Journal of Paleolimnology, 9(3), 195-208.

Rose, N. L., & Juggins, S. (1994). A spatial relationship between carbonaceous particles in lake sediments and sulphur deposition. Atmospheric Environment, 28(2), 177-183.

Ritson, P. I., Bouse, R. M., Flegal, A. R., & Luoma, S. N. (1999). Stable lead isotopic analyses of historic and contemporary lead contamination of San Francisco Bay estuary. Marine Chemistry, 64(1-2), 71-83.

Sanderson, E. W., Ustin, S. L., & Foin, T. C. (2000). The influence of tidal channels on the distribution of salt marsh plant species in Petaluma Marsh, CA, USA. Plant Ecology, 146(1), 29-41.

Sanderson, E. W., Foin, T. C., & Ustin, S. L. (2001). A simple empirical model of salt marsh plant spatial distributions with respect to a tidal channel network. Ecological Modelling, 139(2-3), 293-307.

Shahid, M., Ferrand, E., Schreck, E., & Dumat, C. (2013). Behavior and impact of zirconium in the soil–plant system: plant uptake and phytotoxicity. In Reviews of Environmental Contamination and Toxicology Volume 221 (pp. 107-127). Springer New York.

Smith, R. A., Alexander, R. B., & Wolman, M. G. (1987). Water-quality trends in the nation's rivers. Science, 235(4796), 1607-1615.

Strzyszcz, Z. (1993). Magnetic susceptibility of soils in the areas influenced by industrial emissions. In Soil monitoring (pp. 255-269). Birkhäuser, Basel.

Stuiver, M., Reimer, P.J., and Reimer, R.W., 2018, CALIB 7.1 [WWW program] at http://calib.org, accessed 2018-5-25

The Southern Sonoma County Resource Conservation District (SSCRCD). (1999, July). Petaluma Watershed Enhancement Plan. Retrieved from: http://www.sscrcd.org/watershed-petaluma-river.php.

Thompson, R., & Battarbee, R. (1975). Magnetic susceptibility of lake sediments. Limnology and …, 20(5), 687–698. Retrieved from http://www.jstor.org/stable/10.2307/2834952

Thompson, R., & Oldfield, F. (1986). 1986: Environmental magnetism. London: Allen and Unwin.

Thistlethwaite, R., & Dunlop, J. (2015). The New Livestock Farmer: The Business of Raising and Selling Ethical Meat. Chelsea Green Publishing.

Trowbridge, P. R., Davis, J. A., Mumley, T., Taberski, K., Feger, N., Valiela, L., ... & Coleman, J. (2016). The regional monitoring program for water quality in San Francisco Bay, California, USA: Science in support of managing water quality. Regional Studies in Marine Science, 4, 21-33.

Valette-Silver, N. J. (1993). The use of sediment cores to reconstruct historical trends in contamination of estuarine and coastal sediments. Estuaries, 16(3), 577-588.

Varekamp, J. C. (1991). Trace element geochemistry and pollution history of mudflat and marsh sediments from the Connecticut coastline. Journal of Coastal Research, 105-123.

Watson, E. B., & Byrne, R. (2013). Late Holocene Marsh Expansion in Southern San Francisco Bay, California. Estuaries and coasts, 36(3), 643-653.

Walker, R. (2001). Industry builds the city: The suburbanization of manufacturing in the San Francisco Bay Area, 1850–1940. Journal of Historical Geography, 27(1), 36-57.

Wells, L. E., Goman, M., & Byrne, R. (1997). Long term variability of fresh water flow into the San Francisco Estuary using paleoclimatic methods.

Williams, T. P., Bubb, J. M., & Lester, J. N. (1994). Metal accumulation within salt marsh environments: a review. Marine pollution bulletin, 28(5), 277-290.

Zhang, X., Wang, H., He, L., Lu, K., Sarmah, A., Li, J., ... & Huang, H. (2013). Using biochar for remediation of soils contaminated with heavy metals and organic pollutants. Environmental Science and Pollution Research, 20(12), 8472-8483.